Article

De Novo Design of Phototheranostic Sensitizers based on "Structure-inherent Targeting" for Enhanced Cancer Ablation

Mingle Li, Saran Long, Yao Kang, Lianying Guo, Jingyun Wang, Jiangli Fan, Jianjun Du, and Xiaojun Peng

J. Am. Chem. Soc., **Just Accepted Manuscript** • DOI: 10.1021/jacs.8b09117 • Publication Date (Web): 31 Oct 2018

De Novo Design of Phototheranostic Sensitizers based on "Structure-inherent Targeting" for Enhanced Cancer Ablation

Mingle Li,[†] Saran Long,[†] Yao Kang,[†] Lianying Guo,[‡] Jingyun Wang,[||] Jiangli Fan,[†] Jianjun Du,[†] and Xiaojun Peng*[,†]

[†]State Key Laboratory of Fine Chemicals, Dalian University of Technology, Dalian 116024, China

[‡]Department of Pathophysiology, Dalian Medical University, Dalian 116044, China

[||]Department School of Life Science and Biotechnology, Dalian University of Technology, Dalian 116024, China

ABSTRACT: Structure-inherent targeting (SIT) agents are of particular importance for clinical precision medicine; however, there still exists a great lack of SIT phototheranostics for simultaneous cancer diagnosis and targeted photodynamic therapy (PDT). Herein, for the first time, we propose a "one-for-all" strategy by using Forster Resonance Energy Transfer (FRET) mechanism to construct such omnipotent SIT phototheranostics. Of note, this novel tactic can not only endow conventional sensitizers with highly effective native tumor targeting potency, but also simultaneously improve their photosensitization activities, resulting in dramatically boosted therapeutic index. After intravenous injection of the prepared SIT theranostic, the neoplastic sites are distinctly "lighted up" and distinguished from neighboring tissues, showing a NIR signal-to-background ratio value as high as 12.5. More importantly, benefiting from the FRET effect, markedly amplified light-harvesting ability and $^1O_2$ production are demonstrated. Better still, other favorable features are also simultaneously achieved, including specific mitochondria anchoring, augmented cellular uptake (> 13-fold), as well as ideal biocompatibility, all of which allows orders-of-magnitude promotion in anticancer efficiency both *in vitro* (> 56-fold) and *in vivo* (> 16-fold). We believe this "one-for-all" SIT platform will provide a new idea for future cancer precision therapy.

INTRODUCTION

The problem of severe side effects of current "one-size-fits-all" diagnostic and therapeutic protocols in clinical cancer treatment stimulates the development of "precision medicine" with the purpose of maximizing therapeutic index while minimizing untoward sufferings.[1,2] As a typical photon-triggered therapeutic modality, photodynamic therapy (PDT) has attracted increasing attention in recent years,[3-6] while several factors seriously compromise the PDT clinical practice, especially the poor selectivity towards malignant tissues.[7-9] To achieve accurate PDT, current strategies mainly rely on nanoparticle-mediated delivery systems based on enhanced permeability and retention (EPR) effects,[10,11] and biological conjugation with target ligands (e.g., transferrin,[12] peptide cRGD,[13] biotin,[3] and trastuzumab[14]). However, growing clinical and experimental data suggest that even in the ideal case only a relatively small fraction of injected biologics can finally reach their parenchymal targets,[15,16] such as 1 to 10 parts per 100,000 for antibody conjugates[15,17,18] and ~0.7% for nanoparticles.[19,20] Moreover, the multistep covalent conjugations may alter the conformation, steric freedom, and orientation of target ligands, inevitably compromising their binding abilities.[21,22]

As an ideal alternative, structure-inherent targeting (SIT),[23] namely, the inherent chemical structures of compounds own native targeting potency for interested lesions,[23] offers a new opportunity to realize targeting delivery. This SIT strategy eliminates the need of conjugations. Over the years, SIT molecules have been widely used in Fluorescence-Assisted Resection and Exploration (FLARE) imaging,[24-26] and have been known as excellent contrast agents to visualize sensitive endogenous tissues such as thyroid gland and cartilage.[27-30] However, up to now, their application markedly focus on bio-imaging, rare SIT theranostics combining cancer precision diagnosis and targeted therapy in one component have been designed and utilized for cancer PDT. And also, accesses to obtain SIT agents are overwhelmingly concentrated on combinatorial screening,[26,30] which is time consuming, laborious, and inefficient. Undoubtedly, seeking a more smart and facile approach to construct potent SIT theranostics will provide huge benefits for clinical translation

Notably, for better cancer PDT, besides selectivity to carcinomas, superior optical and physicochemical properties (e.g., relatively strong absorption and high $^1O_2$ quantum yield), specific subcellular organelle-targeting, excellent biocompatibility, and high cellular uptake are also required for photosensitizers (PSs).[31-34] Unfortunately, most conventional PSs can hardly reach these requirements. Taking

phthalocyanine,[35,36] porphyrin,[37] and bodipy PSs as examples,[38,39] they are usually hydrophobic and easy to aggregate in physiological environments, leading to limited membrane permeability and cell uptake. While for cyanine chromophores[40-43] and AIE gens,[44,45] due to the improper triplet state (T_1) energy levels or short T_1 lifetimes, their singlet-to-triplet intersystem crossing (ISC) are inefficient; this badly impedes the subsequent $^1O_2$ generation. Although strategies including structural modification with spin convertor[46] or hydrophilic capping polymers,[47,48] as well as encapsulation within inorganic/metallic materials can mitigate these problems,[49-51] potential limitations still remain, for instance, low drug loading efficiency, accumulation mainly in reticuloendothelial organs, unknown systemic toxicity of exogenous materials, and more.[52,53] Regarding these concerns, we are motivated to develop a "one-for-all" tool that can not only solve these dilemmas, but also simultaneously achieve SIT features in single one small molecule.

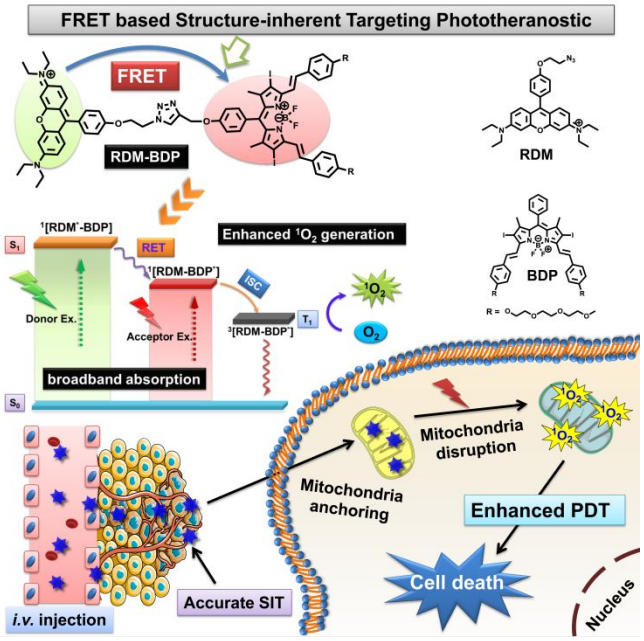

Figure 1. Schematic illustration of FRET mechanism based SIT phototheranostic (RDM-BDP) for amplified $^1O_2$ generation, native tumor targeting, as well as light-triggered enhanced tumor PDT.

Herein, for the first time, we proposed an innovative strategy for using Forster Resonance Energy Transfer (FRET) mechanism to devise robust SIT phototheranostics for significantly amplifying the therapeutic outcome. Previous studies have revealed that cancer cells possess higher magnitude of membrane potential than normal cells, and compounds with permanently delocalized positive charge such as rhodamine derivatives have larger degree of preferential accumulation and retention within tumors.[54-56] In addition, FRET theory has been extensively applied in triplet PSs development aiming at enlarging the photon utility and concomitant $^1O_2$ generation,[37,57] because for most existing photoactive agents, there are only one major absorption profile, leading to their light harvesting capacity disappointed.[57] Inspired by these, we wonder if it was possible that cationic chromophores simultaneously act as SIT sponsors to endow common PSs with native tumor targeting ability, and as energy donors to tailor the photosensitization activities of PSs through FRET mechanism, as a result, markedly improving the anticancer precision and efficiency. As a proof of concept, a representative cationic rhodamine moiety (RDM) was used as energy donor to pair up with a PS example, diiodo-distyryl-bodipy (BDP), to induce the FRET process. As depicted in Figure 1, our strategy successfully endowed the resultant SIT theranostic (RDM-BDP) with great tumor targeting, showing a NIR signal-to-background ratio as high as 12.5. Importantly, due to the FRET effect, RDM-BDP achieved distinctly broader absorption and intensified $^1O_2$ production. Better still, multiple favorable properties were also noted, including specific mitochondria anchoring, promoted cellular uptake (> 13-fold), and ideal biocompatibility. Finally, these merits successfully resulted in significantly enhanced therapeutic response both *in vitro* and *in vivo*. As far as we know, this is the first demonstration of "one-for-all" FRET-based SIT theranostic for cancer precision therapy.

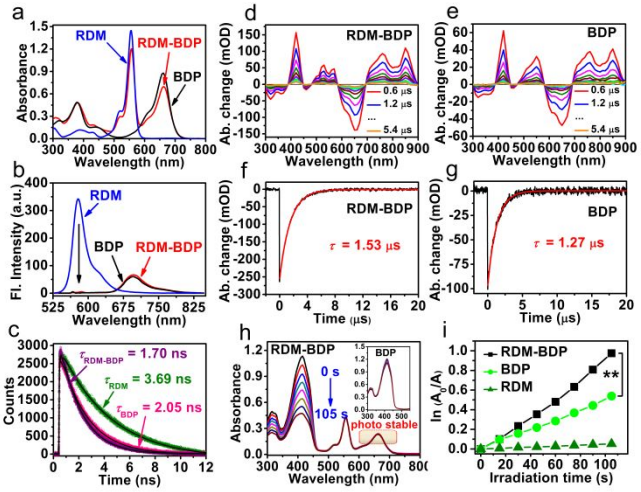

Figure 2. (a) Absorption spectra, (b) fluorescence spectra, (c) fluorescence decay curves of RDM, BDP, and RDM-BDP. Nanosecond time-resolved transient difference absorption spectra of (d) RDM-BDP and (e) BDP in deaerated DCM after pulsed excitation, λ_{ex} = 532 nm. Decay traces of (f) RDM-BDP and (g) BDP at 650 nm in DCM. (h) Photo-degradation curves of DPBF in the presence of RDM-BDP (inset: BDP) under 550 nm irradiation. (i) Comparison of DPBF decomposition rates at 415 nm as a function of irradiation time under panchromatic light illumination.

RESULTS AND DISCUSSION

Synthesis and Spectroscopic Properties. As detailed in Scheme S1, RDM-BDP was synthesized and, to better understand our concept, BDP lacking RDM unit was prepared as control. All structures were fully characterized by ^1H NMR, ^{13}C NMR, and ESI-MS (Figure S1-S12). From the UV-Vis absorbance spectra in Figure 2a, it could be seen that both RDM-BDP and BDP displayed a typical Q band in the range

of 600-700 nm, whereas RDM-BDP possessed an additional intense absorption peak centered at 557 nm which belonged to the RDM moiety. That was to say RDM-BDP achieved a much broader absorption, suggesting a stronger light-harvesting ability as compare to free BDP. Upon 568 nm excitation, the fluorescence of RDM-BDP at 575 nm was completely quenched, showing 129-fold weaker than that of RDM (Figure 2b). Meanwhile, the fluorescence lifetime of RDM-BDP was also shorter than that of RDM, further proving that efficient energy transfer had taken place in RDM-BDP (Figure 2c). Moreover, the nanosecond time-resolved transient difference absorption spectra demonstrated that the transient features of RDM-BDP were similar to that of BDP (Figure 2d-2g), indicating FRET effect did not interfere with the distribution of T_1, and the T_1 of RDM-BDP was predominantly distributed on the energy acceptor unit BDP, but not on the RDM moiety.

$^1O_2$ Generation Ability. To determine whether the broadband absorption facilitates to enhance the $^1O_2$ generation, we firstly used 550 nm and 660 nm as the representative wavelengths of energy donor and acceptor in the following studies, respectively. The measurement mechanism of DPBF for $^1O_2$ was illustrated in Figure S13. As indicated by the DPBF decolorization curves, irradiation of RDM-BDP and BDP with 660 nm light source leaded to a comparable $^1O_2$ generation (Figure S14). However, when they were exposed to 550 nm light, the decrease of DPBF absorbance at 415 nm caused by RDM-BDP was ≈59% in 105 s, while there was almost no decrease for BDP (Figure 2h), suggesting much better $^1O_2$ generation capacity of RDM-BDP than BDP. According to the decay curves of DPBF, the $^1O_2$ yield of RDM-BDP was 9-fold higher than that of BDP (Figure S15). To further understand our concept, a panchromatic light source (400-700 nm) was used for photoexcitation. As expect, the $^1O_2$ generation of RDM-BDP was greatly better than that of BDP (Figure 2i and S16). Moreover, the phosphorescence emission spectrum around 1270 nm validated the $^1O_2$ production again (Figure S17). Hence, FRET effect clearly manipulated the photophysical properties of RDM-BDP, giving rise to an elevated photon utilization as well as boosted $^1O_2$ generation, which were critically important for killing tumor cells during PDT.

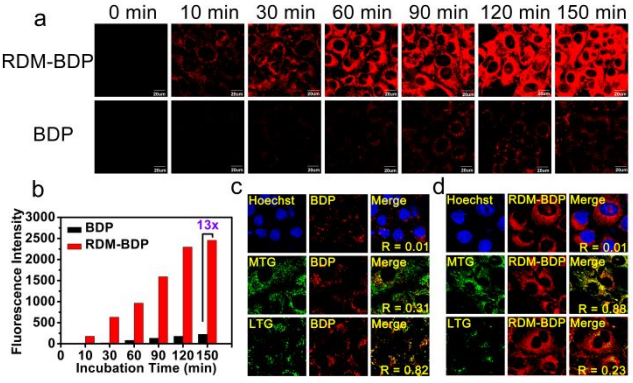

Figure 3. (a) The cellular uptake of RDM-BDP and BDP in 4T1 cells. (b) Intracellular average fluorescence intensity at different time points after incubation with BDP or RDM-BDP. Subcellular colocalization images of (c) BDP and (d) RDM-BDP with Hoechst 33342 (Hoechst), MitoTracker Green (MTG), and LysoTracker Green (LTG) in 4T1 cells, R is the correlation coefficient.

Cellular Uptake and Subcellular Colocalization. Then, we proceeded to investigate whether our strategy enabled to improve the cellular uptake. As displayed in Figure 3a, RDM-BDP could rapidly internalize the tumor cells, and the fluorescence intensity of RDM-BDP in cells after 150 min incubation was 13-fold larger than that of BDP (Figure 3b), revealing noticeably improved cellular uptake was obtained for RDM-BDP. This might be attributed to RDM unit to a certain extent because of larger membrane potential of cancer cell allowing more preferential transport and retention of lipophilic cationic agents.[54] Another item worth noting was that, compared to the typical lysosome localization of BDP (Pearson's coefficient 0.82), the red signals of RDM-BDP was nicely coincident with the green fluorescence of mitochondrial tracking dye (Pearson's coefficient 0.88) (Figure 3c and 3d). Since intracellular mitochondria are more susceptible to toxic $^1O_2$ than other organelles, and mitochondria targeted PSs have more interesting to trigger cell apoptosis,[43,58,59] we speculated that the specific mitochondrial anchoring together with distinctly improved cellular uptake of RDM-BDP would markedly maximized the PDT outcome.

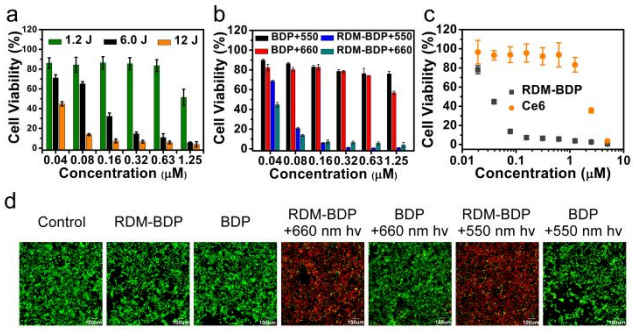

Figure 4. (a) Cell viability of 4T1 cells against various light- and RDM-BDP-dose. (b) Cell viability of 4T1 cells treated with BDP or RDM-BDP at various doses under 550/660 nm light irradiation (12 J/cm^2). (c) PDT efficacy of RDM-BDP and Ce6 in 4T1 cells after 660 nm illumination (12 J/cm^2). (d) Calcein AM and Propidium Iodide co-staining fluorescence imaging in 4T1 cells.

***In Vitro* Light-induced Cellular Toxicity Evaluation.** As expected, RDM-BDP indeed displayed a superior inhibition of cell growth in a concentration- and light dose-dependent manner (Figure 4a), whereas no toxicity was observed in the absence of irradiation (Figure S18). With 12 J/cm^2 light irradiation (660 nm), the half maximal inhibitory concentration (IC_{50}) of RDM-BDP was merely 0.036 μM, but the data was as high as 2.02 μM for BDP, suggesting greatly enhanced PDT potency of RDM-BDP by about 56-fold (Figure 4b). Interestingly, when 4T1 cells were exposed to 550 nm light source, almost no cells were killed by BDP in all doses, in

contrast, RDM-BDP still resulted in a striking photoactive cell damage with an 81-fold enhancement (IC_{50} = 0.055 μM for RDM-BDP *vs.* IC_{50} = 4.45 μM for BDP). Similarly, such encouraging results were also demonstrated in panchromatic light-treated cells (Figure S19), revealing the enhanced light-harvesting potency resulting from FRET effect indeed improved the PDT outcome in essence. In fact, RDM-BDP even was much more outstanding than the widely used clinical PS (Ce6) which has an IC_{50} value of ca. 1.8 μM, 50-fold higher than RDM-BDP (Figure 4c). To the best of our knowledge, RDM-BDP demonstrated the lowest IC_{50} value of bodipy-based PSs reported to date in cellular PDT study.[60] The live/dead cell co-staining data in Figure 4d intuitively demonstrated the robust PDT ability of RDM-BDP again, as revealed by the intense homogeneous red fluorescence for dead cells. All of these results confirmed that our strategy enabled to greatly improve the *in vitro* therapeutic action.

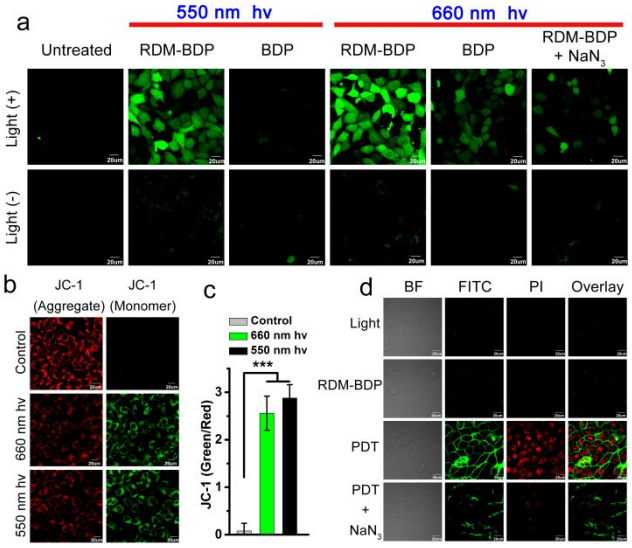

Figure 5. (a) Evaluation of $^1O_2$ generation in 4T1 cells. (b) Mitochondrial membrane potential assay for RDM-BDP-mediated photodamage of mitochondria. (c) The JC-1 monomer to aggregate (green/red) ratio. (d) Confocal fluorescence images of Annexin V-FITC/PI stained 4T1 cells.

Therapeutic Mechanism of RDM-BDP-mediated PDT. To obtain insights into the potential therapeutic mechanism down to subcellular level, the cellular $^1O_2$ was evaluated by using the ROS probe 2, 7-dichlorodihydrofluorescein diacetate (DCFH-DA) (Figure 5a). Compared to control group, in the presence of 660 nm illumination, the RDM-BDP-treated 4T1 cells displayed obviously green fluorescence, indicating an effective ROS generation. Contrarily, relatively dim ROS signals were observed in BDP-treated cells mainly because of its limited cellular uptake. Notably, with 550 nm light irradiation, for RDM-BDP, the ROS generation was also 16 times better than BDP, matching well with the MTT results. Moreover, the ROS induced by RDM-BDP was completed scavenged by NaN_3 (a widely accepted $^1O_2$ scavenger),[9] further implying the produced ROS was $^1O_2$. Since RDM-BDP localized in cellular mitochondria, we envisioned that the generated $^1O_2$ would severely disrupt the mitochondria integrity and initiate cell apoptosis. Remarkably, the JC-1 staining for mitochondria membrane potential showed that, no matter upon 660 nm or 550 nm irradiation, RDM-BDP leaded to severe mitochondrial depolarization as depicted by the increase of green fluorescence signals (Figure 5b, c), subsequently resulting in serious apoptotic cell death (Figure 5d). Similarly, with the addition of NaN_3, 4T1 cells were efficiently prevented from the fate of death, suggesting the cell death was really induced by generated $^1O_2$. Contrarily, BDP only caused slightly lysosome dysfunction (Figure S20) and early cell apoptosis (Figure S21).

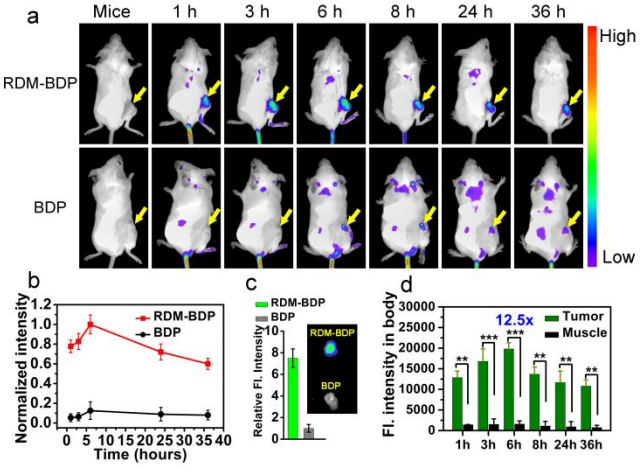

Figure 6. (a) *In vivo* fluorescence imaging of 4T1 tumor-bearing BALB/c mice after intravenous injection of BDP and RDM-BDP. (b) Normalized fluorescence intensity of BDP and RDM-BDP in tumor sites at different time points. (c) The *ex vivo* tumor fluorescence imaging after 36 h injection of RDM-BDP and BDP. (d) Relative fluorescence change in the tumor and adjacent muscle tissues for RDM-BDP-administrated mice.

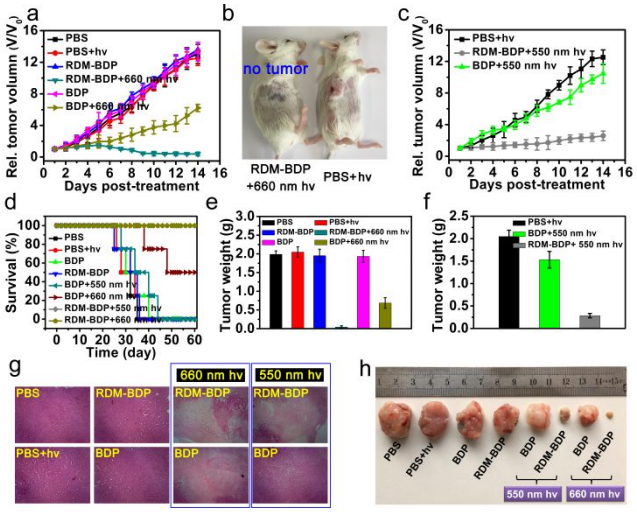

Figure 7. (a) Relative tumor volume changes in tumor-bearing mice during the treatments (660 nm irradiation). (b)

Representative photos of mice at the 14th day. (c) Relative tumor volume in the mice after different treatments (550 nm irradiation). (d) Survival curves of mice in different groups during the 60 day evaluation. (e, f) Tumor weight, (g) H&E staining of tumor slices, (h) representative tumor images from different groups of tumor-bearing mice.

Structure-Inherent Targeting Ability of RDM-BDP. To evaluate the SIT performance of RDM-BDP, the BALB/c mice bearing a subcutaneous 4T1 tumor was intravenously injected with 8 nmol RDM-BDP, followed by *in vivo* fluorescence imaging at different time points. Encouragingly, very appealing spontaneous tumor targeting was displayed (Figure 6a). Only 1 hour after injection, the tumor site could be clearly "lighted up" and distinguished from neighboring tissues. With time increasing, the fluorescence intensity at tumor site was gradually enhanced (Figure 6b), reaching the maximum at 6 h post-injection (p.i.), while nearly no fluorescence signals were observed in BDP-injected mice. The representative *ex vivo* tumor image further demonstrated the more efficient tumor-specific uptake and retention of RDM-BDP than BDP (Figure 6c). Significantly, RDM-BDP exhibited a SBR value (calculated from the difference in fluorescence intensity between tumor and surrounding muscle) up to 12.5 (Figure 6d), whereas previously, such SBR value in a tumor more than 2.5 was regarded as substantially preferential accumulation,[27-30] highlighting the advantages of our SIT platform in terms of tumor targeting and diagnose, and suggesting that RDM-BDP enabled to confine the PDT on tumor regions so as to reduce the side effects on normal tissues.

***In Vivo* Anticancer Effect on Tumor Growth and Biosafety Evaluation.** For *in vivo* cancer therapy (Figure 7a), tumors in the mice treated with PBS followed by 660 nm irradiation increased rapidly with an ca. 14 fold increment, similar to that treated with PBS alone, excluding the influence of NIR irradiation on tumor inhibition. Owing to the negligible dark toxicity, free RDM-BDP and BDP also showed no tumor suppression. After 660 nm irradiation, RDM-BDP resulted in an extraordinary tumor regression with no tumor relapse; however, only slight tumor inhibition was observed for mice administrated with BDP. Meanwhile, the tumor sizes of BDP irradiation mice were about 16 times larger than that of RDM-BDP irradiation mice at the end of observation period. Besides, the thorough tumor eradication further proved the robust *in vivo* PDT efficacy of RDM-BDP (Figure 7b). For 550 nm light irradiation, the tumors in BDP group still grew rapidly, whereas RDM-BDP completely inhibited the tumor growth (Figure 7c), which meaning superb *in vivo* anticancer outcome could be obtained by broadband absorption as the result of FRET effect. Also, RDM-BDP successfully enhanced the survival time of mice (Figure 7d). The superior antitumor performance of RDM-BDP was further manifested by the average tumor weights (Figure 7e and 7f) as well as hematoxylin & eosin (H&E) staining of tumor slices (Figure 7g), and the representative tumor photographs provided intuitive evidence (Figure 7h). Fortunately, no abnormal body weight change was found in all mice (Figure S22) and also, there was no substantial damage or distinct inflammation lesions in all normal organs including heart, liver, spleen, lung, and kidney (Figure S23), suggesting the low *in vivo* toxicities of various treatments in this work and that RDM-BDP was suitable for *in vivo* application.

CONCLUSION

In summary, we have developed a novel approach based on intramolecular FRET mechanism to design SIT theranostic for precise light-triggered tumor treatment. In particular, RDM-BDP operated based on FRET mechanism and significantly elevated the light-harvesting ability as well as $^1O_2$ generation. *In vivo* tumor fluorescence imaging study clearly confirmed that RDM-BDP could spontaneously accumulate within tumor site and exhibited a fairly high SBR value, enabling the tumor and its margins easily visualized and proving the potential for precise imaging-guided tumor PDT. Furthermore, RDM-BDP could specifically target to mitochondria, and substantially enhanced the internalization in cancer cells. These features thereby markedly maximized the PDT effect on tumors. More importantly, this unconventional strategy can be readily adopted for improving the therapeutic performance of other existing photoactive agents, such as phthalocyanines and porphyrins. We believe that our FRET-based SIT PS development platform will provide considerable advantages for cancer diagnostic and therapeutic.

ASSOCIATED CONTENT

Supporting Information. Detailed experimental conditions and methods, Scheme S1 and Figures S1-S23.

AUTHOR INFORMATION

Corresponding Author

*pengxj@dlut.edu.cn

Notes

The authors declare no competing financial interests.

ACKNOWLEDGEMENTS

This work was supported by National Science Foundation of China (project 21421005, 21576037, and U1608222).

REFERENCES

(1) Li, X.; Kim, J.; Yoon, J.; Chen, X. Cancer-Associated, Stimuli-Driven, Turn on Theranostics for Multimodality Imaging and Therapy. *Adv. Mater.* **2017**, *29*, 1606857.

(2) Collins, D. C.; Sundar, R.; Lim, J. S. J.; Yap, T. A. Towards Precision Medicine in the Clinic: From Biomarker Discovery to Novel Therapeutics. *Trends Pharmacol. Sci*. **2017**, *38*, 25-40.

(3) Li, M.; Xia, J.; Tian, R.; Wang, J.; Fan, J.; Du, J.; Long, S.; Song, X.; Foley, J. W.; Peng, X. Near-Infrared Light-Initiated Molecular Superoxide Radical Generator: Rejuvenating Photodynamic Therapy against Hypoxic Tumors. *J. Am. Chem. Soc.* **2018**, DOI:10.1021/jacs.8b08658.

(4) Fan, W.; Huang, P.; Chen, X. Overcoming the Achilles' heel of photodynamic therapy. *Chem. Soc. Rev.* **2016**, *45*, 6488-6519.

(5) Dolmans, D. E. J. G. J.; Fukumura, D.; Jain, R. K. Photodynamic therapy for cancer. *Nat. Rev. Cancer* **2003**, *3*, 380.

(6) Li, X.; Lee, S.; Yoon, J. Supramolecular photosensitizers rejuvenate photodynamic therapy. *Chem. Soc. Rev.* **2018**, *47*, 1174-1188.

(7) Li, X.; Kolemen, S.; Yoon, J.; Akkaya Engin, U. Activatable Photosensitizers: Agents for Selective Photodynamic Therapy. *Adv. Funct. Mater.* **2016**, *27*, 1604053.

(8) Luo, G.-F.; Chen, W.-H.; Hong, S.; Cheng, Q.; Qiu, W.-X.; Zhang, X.-Z. A Self-Transformable pH-Driven Membrane-Anchoring Photosensitizer for Effective Photodynamic Therapy to Inhibit Tumor Growth and Metastasis. *Adv. Funct. Mater.* **2017**, *27*, 1702122.

(9) Zhao, X.; Li, M.; Sun, W.; Fan, J.; Du, J.; Peng, X. An estrogen receptor targeted ruthenium complex as a two-photon photodynamic therapy agent for breast cancer cells. *Chem. Commun*. **2018**, *54*, 7038-7041.

(10) Blanco, E.; Shen, H.; Ferrari, M. Principles of nanoparticle design for overcoming biological barriers to drug delivery. *Nat. Biotechnol.* **2015**, *33*, 941.

(11) Duncan, R.; Richardson, S. C. W. Endocytosis and Intracellular Trafficking as Gateways for Nanomedicine Delivery: Opportunities and Challenges. *Mol. Pharm.* **2012**, *9*, 2380-2402.

(12) Goswami, U.; Dutta, A.; Raza, A.; Kandimalla, R.; Kalita, S.; Ghosh, S. S.; Chattopadhyay, A. Transferrin-Copper Nanocluster-Doxorubicin Nanoparticles as Targeted Theranostic Cancer Nanodrug. *ACS Appl. Mater. Inter.* **2018**, *10*, 3282-3294.

(13) Choi, H. S.; Gibbs, S. L.; Lee, J. H.; Kim, S. H.; Ashitate, Y.; Liu, F.; Hyun, H.; Park, G.; Xie, Y.; Bae, S.; Henary, M.; Frangioni, J. V. Targeted zwitterionic near-infrared fluorophores for improved optical imaging. *Nat. Biotechnol.* **2013**, *31*, 148.

(14) Mitsunaga, M.; Ogawa, M.; Kosaka, N.; Rosenblum, L. T.; Choyke, P. L.; Kobayashi, H. Cancer cell-selective *in vivo* near infrared photoimmunotherapy targeting specific membrane molecules. *Nat. Med.* **2011**, *17*, 1685.

(15) Ferrari, M. Cancer nanotechnology: opportunities and challenges. *Nat. Rev. Cancer* **2005**, *5*, 161.

(16) Jeong, Y.; Jo, Y. K.; Kim, B. J.; Yang, B.; Joo, K. I.; Cha, H. J. Sprayable Adhesive Nanotherapeutics: Mussel-Protein-Based Nanoparticles for Highly Efficient Locoregional Cancer Therapy. *ACS Nano* **2018**, *12*, 8909-8919.

(17) Wang, X.; Yang, L.; Chen, Z.; Shin Dong, M. Application of Nanotechnology in Cancer Therapy and Imaging. *CA Cancer J Clin.* **2008**, *58*, 97-110.

(18) Li, K. C. P.; Pandit, S. D.; Guccione, S.; Bednarski, M. D. Molecular Imaging Applications in Nanomedicine. *Biomed. Microdevices* **2004**, *6*, 113-116.

(19) Wilhelm, S.; Tavares, A. J.; Dai, Q.; Ohta, S.; Audet, J.; Dvorak, H. F.; Chan, W. C. W. Analysis of nanoparticle delivery to tumours. *Nat. Rev. Mater.* **2016**, *1*, 16014.

(20) Dai, Q.; Wilhelm, S.; Ding, D.; Syed, A. M.; Sindhwani, S.; Zhang, Y.; Chen, Y. Y.; MacMillan, P.; Chan, W. C. W. Quantifying the Ligand-Coated Nanoparticle Delivery to Cancer Cells in Solid Tumors. *ACS Nano* **2018**, *12*, 8423-8435.

(21) Paulos, C. M.; Reddy, J. A.; Leamon, C. P.; Turk, M. J.; Low, P. S. Ligand Binding and Kinetics of Folate Receptor Recycling *in Vivo*: Impact on Receptor-Mediated Drug Delivery. *Mol. Pharmacol.* **2004**, *66*, 1406.

(22) Cheng, Z.; Al Zaki, A.; Hui, J. Z.; Muzykantov, V. R.; Tsourkas, A. Multifunctional Nanoparticles: Cost Versus Benefit of Adding Targeting and Imaging Capabilities. *Science* **2012**, 338, 903.

(23) Hyun, H.; Park, M. H.; Owens, E. A.; Wada, H.; Henary, M.; Handgraaf, H. J. M.; Vahrmeijer, A. L.; Frangioni, J. V.; Choi, H. S. Structure-inherent targeting of near-infrared fluorophores for parathyroid and thyroid gland imaging. *Nat. Med.* **2015**, *21*, 192.

(24) Choi Hak, S.; Nasr, K.; Alyabyev, S.; Feith, D.; Lee Jeong, H.; Kim Soon, H.; Ashitate, Y.; Hyun, H.; Patonay, G.; Strekowski, L.; Henary, M.; Frangioni John, V. Synthesis and *In Vivo* Fate of Zwitterionic Near-Infrared Fluorophores. *Angew. Chem. Int. Edit.* **2011**, *50*, 6258-6263.

(25) Owens Eric, A.; Lee, S.; Choi, J.; Henary, M.; Choi Hak, S. NIR fluorescent small molecules for intraoperative imaging. *WiRes Nanomed. Nanobi.* **2015**, *7*, 828-838.

(26) Owens, E. A.; Hyun, H.; Dost, T. L.; Lee, J. H.; Park, G.; Pham, D. H.; Park, M. H.; Choi, H. S.; Henary, M. Near-Infrared Illumination of Native Tissues for Image-Guided Surgery. *J. Med. Chem.* **2016**, *59*, 5311-5323.

(27) Hyun, H.; Owens Eric, A.; Wada, H.; Levitz, A.; Park, G.; Park Min, H.; Frangioni John, V.; Henary, M.; Choi Hak, S. Cartilage-Specific Near-Infrared Fluorophores for Biomedical Imaging. *Angew. Chem. Int. Edit.* **2015**, *54*, 8648-8652.

(28) Zhao, X.; Li, Y.; Jin, D.; Xing, Y.; Yan, X.; Chen, L. A near-infrared multifunctional fluorescent probe with an inherent tumor-targeting property for bioimaging. *Chem. Commun*. **2015**, *51*, 11721-11724.

(29) Hyun, H.; Wada, H.; Bao, K.; Gravier, J.; Yadav, Y.; Laramie, M.; Henary, M.; Frangioni John, V.; Choi Hak, S. Phosphonated Near-Infrared Fluorophores for Biomedical Imaging of Bone. *Angew. Chem. Int. Edit.* **2014**, *53*, 10668-10672.

(30) Owens, E. A.; Hyun, H.; Tawney, J. G.; Choi, H. S.; Henary, M. Correlating Molecular Character of NIR Imaging Agents with Tissue-Specific Uptake. *J. Med. Chem.* **2015**, *58*, 4348-4356.

(31) Yang, T.; Liu, L.; Deng, Y.; Guo, Z.; Zhang, G.; Ge, Z.; Ke, H.; Chen, H. Ultrastable Near-Infrared Conjugated-Polymer Nanoparticles for Dually Photoactive Tumor Inhibition. *Adv. Mater.* **2017**, *29*, 1700487.

(32) Zhou, Z.; Song, J.; Nie, L.; Chen, X. Reactive oxygen species generating systems meeting challenges of photodynamic cancer therapy. *Chem. Soc. Rev.* **2016**, *45*, 6597-6626.

(33) Li, M.; Peng, X. Research Progress on the Phthalocyanine Based Targeting Photosensitizers in Photodynamic Therapy. *Huaxue Xuebao* **2016**, *74*, 959-968.

(34) Bian, Y.; Li, M.; Fan, J.; Du, J.; Long, S.; Peng, X. A proton-activatable aminated-chrysophanol sensitizer for photodynamic therapy. *Dyes Pigm.* **2017**, *147*, 476-483.

(35) Li, X.; Lee, D.; Huang, J.-D.; Yoon, J. Phthalocyanine-Assembled Nanodots as Photosensitizers for Highly Efficient Type I Photoreactions in Photodynamic Therapy. *Angew. Chem. Int. Edit.* **2018**, *57*, 9885-9890.

(36) Li, X.; Kim, C. y.; Lee, S.; Lee, D.; Chung, H.-M.; Kim, G.; Heo, S.-H.; Kim, C.; Hong, K.-S.; Yoon, J. Nanostructured Phthalocyanine Assemblies with Protein-Driven Switchable Photoactivities for Biophotonic Imaging and Therapy. *J. Am. Chem. Soc.* **2017**, 139, 10880-10886.

(37) Zheng, X.; Wang, L.; Liu, S.; Zhang, W.; Liu, F.; Xie, Z. Nanoparticles of Chlorin Dimer with Enhanced Absorbance for Photoacoustic Imaging and Phototherapy. *Adv. Funct. Mater.* **2018**, *28*, 1706507.

(38) Jung, H. S.; Han, J.; Shi, H.; Koo, S.; Singh, H.; Kim, H.-J.; Sessler, J. L.; Lee, J. Y.; Kim, J.-H.; Kim, J. S. Overcoming the Limits of Hypoxia in Photodynamic Therapy: A Carbonic Anhydrase IX-Targeted Approach. *J. Am. Chem. Soc.* **2017**, *139*, 7595-7602.

(39) Li, M.; Tian, R.; Fan, J.; Du, J.; Long, S.; Peng, X. A lysosome-targeted BODIPY as potential NIR photosensitizer for photodynamic therapy. *Dyes Pigm.* **2017**, 147, 99-105.

(40) Huang, H.; Long, S.; Li, M.; Gao, F.; Du, J.; Fan, J.; Peng, X. Bromo-pentamethine as mitochondria-targeted photosensitizers for cancer cell apoptosis with high efficiency. *Dyes Pigm.* **2018**, *149*, 633-638.

(41) Jung, H. S.; Lee, J.-H.; Kim, K.; Koo, S.; Verwilst, P.; Sessler, J. L.; Kang, C.; Kim, J. S. Mitochondria-Targeted Cryptocyanine-Based Photothermogenic Photosensitizer. *J. Am. Chem. Soc.* **2017**, *139*, 9972-9978.

(42) Luo, S.; Tan, X.; Fang, S.; Wang, Y.; Liu, T.; Wang, X.; Yuan, Y.; Sun, H.; Qi, Q.; Shi, C. Mitochondria-Targeted Small-Molecule Fluorophores for Dual Modal Cancer Phototherapy. *Adv. Funct. Mater.* **2016**, *26*, 2826-2835.

(43) Noh, I.; Lee, D.; Kim, H.; Jeong, C. U.; Lee, Y.; Ahn, J. O.; Hyun, H.; Park, J. H.; Kim, Y. C. Enhanced Photodynamic Cancer Treatment by Mitochondria-Targeting and Brominated Near-Infrared Fluorophores. *Adv. Sci.* **2017**, *5*, 1700481.

(44) Chen, C.; Song, Z.; Zheng, X.; He, Z.; Liu, B.; Huang, X.; Kong, D.; Ding, D.; Tang, B. Z. AIEgen-based theranostic system: targeted imaging of cancer cells and adjuvant amplification of antitumor efficacy of paclitaxel. *Chem. Sci.* **2017**, *8*, 2191-2198.

(45) Yu, C. Y. Y.; Xu, H.; Ji, S.; Kwok, R. T. K.; Lam, J. W. Y.; Li, X.; Krishnan, S.; Ding, D.; Tang, B. Z. Mitochondrion-Anchoring Photosensitizer with Aggregation-Induced Emission Characteristics Synergistically Boosts the Radiosensitivity of Cancer Cells to Ionizing Radiation. *Adv. Mater.* **2017**, *29*, 1606167.

(46) Yang, T.; Liu, L.; Deng, Y.; Guo, Z.; Zhang, G.; Ge, Z.; Ke, H.; Chen, H. Ultrastable Near-Infrared Conjugated-Polymer Nanoparticles for Dually Photoactive Tumor Inhibition. *Adv. Mater.* **2017**, *29*, 1700487.

(47) Dong, Z.; Feng, L.; Hao, Y.; Chen, M.; Gao, M.; Chao, Y.; Zhao, H.; Zhu, W.; Liu, J.; Liang, C.; Zhang, Q.; Liu, Z. Synthesis of Hollow Biomineralized $CaCO_3$-Polydopamine Nanoparticles for Multimodal Imaging-Guided Cancer Photodynamic Therapy with Reduced Skin Photosensitivity. *J. Am. Chem. Soc.* **2018**, *140*, 2165-2178.

(48) Wang, D.; Liu, B.; Ma, Y.; Wu, C.; Mou, Q.; Deng, H.; Wang, R.; Yan, D.; Zhang, C.; Zhu, X. A Molecular Recognition Approach To Synthesize Nucleoside Analogue Based Multifunctional Nanoparticles for Targeted Cancer Therapy. *J. Am. Chem. Soc.* **2017**, *139*, 14021-14024.

(49) Poß, M.; Zittel, E.; Seidl, C.; Meschkov, A.; Muñoz, L.; Schepers, U.; Feldmann, C. A. $Gd_4^{3+}[AlPCS_4]_3^{4-}$ Nanoagent Generating $^1O_2$ for Photodynamic Therapy. *Adv. Funct. Mater.* **2018**, *28*, 1801074.

(50) Lucky, S. S.; Soo, K. C.; Zhang, Y. Nanoparticles in Photodynamic Therapy. *Chem. Rev.* **2015**, *115*, 1990-2042.

(51) Kang, Y.; Sun, W.; Fan, J.; Wei, Z.; Wang, S.; Li, M.; Zhang, Z.; Xie, Y.; Du, J.; Peng, X. Ratiometric real-time monitoring of hydroxyapatite-doxorubicin nanotheranostic agents for on-demand tumor targeted chemotherapy. *Mater. Chem. Front.* **2018**, *2*, 1791-1798.

(52) Chen, F.; Cai, W. Nanomedicine for targeted photothermal cancer therapy: where are we now? *Nanomed. Nanotechnol.* **2015**, *10*, 1-3.

(53) Devarajan, P. V.; Patravale, V. B. Nanomedicine-prospects and challenges. *Drug Deliv. Transl. Re.* **2013**, *3*, 381-381.

(54) Bernal, S. D.; Lampidis, T. J.; Summerhayes, I. C.; Chen, L. B. Rhodamine-123 selectively reduces clonal growth of carcinoma cells *in vitro*. *Science* **1982**, *218*, 1117.

(55) Lampidis, T. J.; Bernal, S. D.; Summerhayes, I. C.; Chen, L. B. Selective Toxicity of Rhodamine 123 in Carcinoma Cells *in Vitro*. *Cancer Res.* **1983**, *43*, 716-720.

(56) Shea, C. R.; Chen, N.; Wimberly, J.; Hasan, T. Rhodamine Dyes as Potential Agents for Photochemotherapy of Cancer in Human Bladder Carcinoma Cells. *Cancer Res.* **1989**, *49*, 3961

(57) Guo, S.; Ma, L.; Zhao, J.; Küçüköz, B.; Karatay, A.; Hayvali, M.; Yaglioglu, H. G.; Elmali, A. BODIPY triads triplet photosensitizers enhanced with intramolecular resonance energy transfer (RET): broadband visible light absorption and application in photooxidation. *Chem. Sci.* **2014**, *5*, 489-500.

(58) Liu, H.-W.; Hu, X.-X.; Li, K.; Liu, Y.; Rong, Q.; Zhu, L.; Yuan, L.; Qu, F.-L.; Zhang, X.-B.; Tan, W. A mitochondrial-targeted prodrug for NIR imaging guided and synergetic NIR photodynamic-chemo cancer therapy. *Chem. Sci.* **2017**, *8*, 7689-7695.

(59) Wen, L.; Zhang, Z.; Yin, Z. K.; Huiran, Y.; Shujuan, L.; Aqiang, X.; Song, G.; Qiang, Z.; Wei, H. A Mitochondria-Targeted Photosensitizer Showing Improved Photodynamic Therapy Effects Under Hypoxia. *Angew. Chem. Int. Edit.* **2016**, *128*, 10101-10105.

(60) Kue, C. S.; Ng, S. Y.; Voon, S. H.; Kamkaew, A.; Chung, L. Y.; Kiew, L. V.; Lee, H. B. Recent strategies to improve boron dipyrromethene (BODIPY) for photodynamic cancer therapy: an updated review. *Photoch. Photobio. Sci.* **2018**, DOI:10.1039/C8PP00113H.

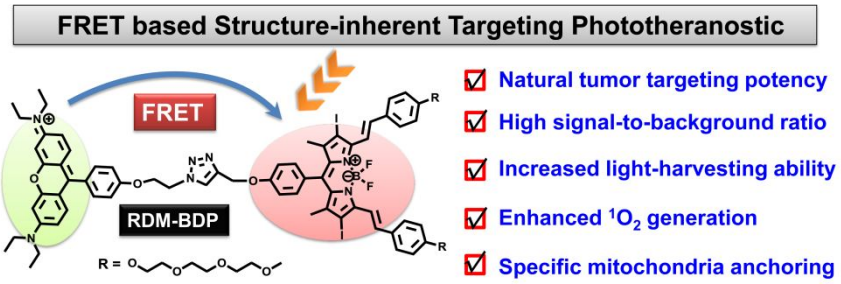
FRET based Structure-inherent Targeting Phototheranostic
FRET
RDM-BDP
R =
Natural tumor targeting potency
High signal-to-background ratio
Increased light-harvesting ability
Enhanced $^1O_2$ generation
Specific mitochondria anchoring